Performance Evaluation of a New Dual-Polarization Microphysical Algorithm Based on Long-Term X-Band Radar and Disdrometer Observations

MARIOS N. ANAGNOSTOU,[*,+] JOHN KALOGIROS,[+] FRANK S. MARZANO,[*,#] EMMANOUIL N. ANAGNOSTOU,[@] MARIO MONTOPOLI,[#,&] AND ERRICO PICCIOTI[#]

[*] *Department of Information Engineering, Sapienza University of Rome, Rome, Italy*
[+] *Institute of Environmental Research and Sustainable Development, National Observatory of Athens, Athens, Greece*
[#] *CETEMPS Centre of Excellence, University of L'Aquila, L'Aquila, Italy*
[@] *Department of Civil and Environmental Engineering, University of Connecticut, Storrs, Connecticut*
[&] *Department of Geography, University of Cambridge, Cambridge, United Kingdom*

(Manuscript received 17 April 2012, in final form 22 October 2012)

ABSTRACT

Accurate estimation of precipitation at high spatial and temporal resolution of weather radars is an open problem in hydrometeorological applications. The use of dual polarization gives the advantage of multiparameter measurements using orthogonal polarization states. These measurements carry significant information, useful for estimating rain-path signal attenuation, drop size distribution (DSD), and rainfall rate. This study evaluates a new self-consistent with optimal parameterization attenuation correction and rain microphysics estimation algorithm (named SCOP-ME). Long-term X-band dual-polarization measurements and disdrometer DSD parameter data, acquired in Athens, Greece, have been used to quantitatively and qualitatively compare SCOP-ME retrievals of median volume diameter D_0 and intercept parameter N_W with two existing rain microphysical estimation algorithms and the SCOP-ME retrievals of rain rate with three available radar rainfall estimation algorithms. Error statistics for rain rate estimation, in terms of relative mean and root-mean-square error and efficiency, show that the SCOP-ME has low relative error if compared to the other three methods, which systematically underestimate rainfall. The SCOP-ME rain microphysics algorithm also shows a lower relative error statistic when compared to the other two microphysical algorithms. However, measurement noise or other signal degradation effects can significantly affect the estimation of the DSD intercept parameter from the three different algorithms used in this study. Rainfall rate estimates with SCOP-ME mostly depend on the median volume diameter, which is estimated much more efficiently than the intercept parameter. Comparisons based on the long-term dataset are relatively insensitive to path-integrated attenuation variability and rainfall rates, providing relatively accurate retrievals of the DSD parameters when compared to the other two algorithms.

1. Introduction

Weather radar can provide spatiotemporal rainfall observations that can support hydrometeorological modeling and flood forecasting. Rain rate retrievals can be estimated from the single polarization radar measurement, that is, the radar reflectivity (Marshall and Palmer 1948; Battan 1973; Atlas and Ulbrich 1990; Joss and Waldvogel 1990) using the traditional standard reflectivity–rainfall (Z–R) relation on a physical basis of additional convective–stratiform rain classification information (Anagnostou and Krajewski 1999). A Z–R relation is obtained by regression analysis of gauge measurements and radar reflectivity or from drop size distributions (DSD) measured by aircraft and in situ disdrometers. However, the standard Z–R relation does not carry enough information to account for the climatological and orographic uniqueness of each location and temporal changes of the DSD. Thus, it cannot provide accurate rainfall rate (R in mm h^{-1}) estimates for different types of storms that are associated with varying microphysical processes.

On the other hand, rainfall rate estimators can be derived from modern polarimetric radar observations, which are related to the DSD in the radar volume

Corresponding author address: Dr. Marios N Anagnostou, Department of Information Engineering, Sapienza University of Rome, Via Eudossiana 18, 00184 Rome, Italy.
E-mail: marios.anagnostou@uniroma1.it; ma111@engr.uconn.edu

DOI: 10.1175/JHM-D-12-057.1

© 2013 American Meteorological Society

(Bringi and Chandrasekar 2001). Dual-polarization (or polarimetric) weather radars have a significant advantage over single-polarization systems because they allow multiparameter measurements using orthogonal polarization states. Polarimetric measurements, apart from the horizontal polarization reflectivity (Z_H in dBZ), usually include the differential reflectivity ($Z_{\rm DR}$ in dB), the differential phase shift ($\Phi_{\rm DP}$ in degrees), and the copolar correlation coefficient (ρ_{HV}, unitless).

Polarization diversity has a significant impact on correcting for rain-path signal attenuation in attenuating frequency (C band and X band) radar measurements, making these systems applicable in heavy precipitation estimation (Testud et al. 2000). The typical range of X-band radar can be short (60–120 km) compared to the long-range operational weather radars [consisting primarily of S-band, like the Weather Surveillance Radar-1988 Doppler (WSR-88D) network in the United States, and C-band radars, like most of the radar networks in Europe], but X-band radar can be low power, mobile, and constitute a cost effective system for filling up gaps in existing national radar networks. Examples include monitoring small-scale basins in mountainous regions and urban areas (Anagnostou et al. 2010; Park et al. 2005) where, owing to the high spatial resolution associated with X-band radars, flood forecasting with distributed hydrologic modeling could be more effectively carried out with high-resolution rainfall forcing (Ogden et al. 2000; Maki et al. 2008). A major drawback in X-band rainfall estimation is the rain-path signal attenuation effect, which can be larger than 10 dB for heavy rain events, causing significant errors in rainfall estimation. The fundamental aspect that brought X-band back to the interest of hydrometeorologists for rainfall estimation is that the copolarization differential phase shift ($\Phi_{\rm DP}$) measurement can be used as a constraint parameter for the effective estimation of specific copolar (A_H), differential ($A_{\rm DP}$), and rain attenuation profiles (Testud et al. 2000; Matrosov et al. 2005; Park et al. 2005; Anagnostou et al. 2009; Marzano et al. 2010).

Based on data from different hydroclimatic regimes, numerous studies have confirmed that the estimation of rain microphysics can be significantly improved by the use of polarimetric radar parameters (Ryzhkov and Zrnić 1996; Anagnostou et al. 2004; Anagnostou et al. 2007; Matrosov et al. 2005; Park et al. 2005; Kim et al. 2010). The method by Gorgucci et al. (2006), which was proposed for C-band, and a more robust algorithm, proposed for S, C, and X band (Gorgucci et al. 2008), can provide an estimate of the two DSD governing parameters, namely, the raindrop median diameter D_0 (mm) and intercept parameter N_W (mm^{-1} m^{-3}) of the assumed normalized gamma distribution, by utilizing power-related radar parameters (Z_H and $Z_{\rm DR}$), the specific differential phase shift $K_{\rm DP}$ (in degrees per kilometer), and the slope parameter β of drop shape (axis ratio r) against rain droplet diameter. Park et al. (2005) adapted a method similar to Gorgucci et al. (2001) at X-band frequencies. Many studies have also proposed the estimation of the DSD parameters as part of rain attenuation correction and/or rain estimation algorithms. The method developed by Testud et al. (2000) provides estimates of N_W for C-band and X-band frequencies using an attenuation correction algorithm, employing the differential phase shift $\Phi_{\rm DP}$ as an external constraint within the attenuation-estimation method, whereas Matrosov et al. (2005) estimated D_0 by relating it with the attenuation-corrected $Z_{\rm DR}$ for X-band. The aforementioned methods are either two- or three-parameter physical-based ad hoc or empirical algorithms. There is also a nonparametric estimation of DSD from slant-profile dual-polarized Doppler spectra observations, presented by Moisseev et al. (2006). Vulpiani et al. (2009) and Anagnostou et al. (2008) have developed a nonparametric approach to estimate the three governing parameters of DSD from S or C band and X-band dual-polarization radar parameters on the basis of a regularized artificial neural network (NN) or a Bayesian approach, respectively.

Recent studies by Anagnostou et al. (2009, 2010) and Kalogiros et al. (2013a) have led to the development and demonstration of a new algorithm for both polarimetric attenuation correction in rain and rain parameter estimation (i.e., rain rate and DSD). Anagnostou et al. (2009, 2010) evaluated a modified ZPHI algorithm (Testud et al. 2000) for attenuation and rainfall estimation with N_W normalization, using observations from mobile X-band dual-polarization radar over complex terrain basins. Kalogiros et al. (2013a,b) showed that the new self-consistent with optimal parameterization (SCOP) attenuation correction and rain microphysics estimation (SCOP-ME) algorithm can provide improved estimates of rain rate and DSD parameters when compared with existing algorithms on the basis of simulated radar data derived from long-term observed raindrop spectra. The objective of this work is to statistically evaluate the performance of the SCOP-ME algorithm using an extensive database of actual X-band dual-polarization observations coincident with in situ measurements from a 2D video disdrometer (2DVD) acquired in Athens, Greece, in a period of four years. The statistical performances of the SCOP-ME algorithm are also evaluated with different rainfall rate and DSD estimation algorithms taken from the literature. The statistical error evaluation of the SCOP-ME algorithm is performed for the horizontal polarization Z_H and

differential Z_{DR} reflectivity observed with the radar and corrected for attenuation in rain against the corresponding radar products calculated from the 2DVD-observed DSD as a function of different path-integrated attenuation (PIA) values in four different categories.

The paper is organized as follows. In section 2 the SCOP-ME algorithm is briefly described. In sections 3 and 4 the results of the quantitative (statistics) and qualitative (test case) comparison of the estimations from the SCOP-ME algorithm and two different rain microphysical estimation (i.e., median volume diameter D_0 and intercept parameter N_W) algorithms, found in the literature, against the disdrometer-observed DSD parameters and three different radar rainfall estimation algorithms, also taken from the literature, are presented. Finally, the conclusions in section 5 summarize the results of this work.

2. Rain microphysics retrieval algorithm

The polarimetric rain microphysics algorithm SCOP-ME for X-band radars was based on relations valid at the theoretical Rayleigh scattering limit corrected by a multiplicative rational polynomial function of reflectivity-weighted raindrop diameter (D_z) to approximate the Mie character of scattering at these electromagnetic frequencies. The reflectivity-weighted mean diameter is given by $D_z = E[D^7]/E[D^6]$ [1], where D is the raindrop equivolume diameter and E stands for the expectation value. The expectation value is estimated in practice as the DSD-weighted integral over the whole range of diameter values. The algorithm was developed from T-matrix scattering simulations (Kalogiros et al. 2013a) for a wide range of DSD parameters, a variable raindrop axis ratio around the relationship given by Beard and Chuang (1987), a Fisher distribution with a circular standard deviation of 7.5° for canting angle distribution, and air temperature varying from 5° to 20°C. The maximum parameterization error of SCOP-ME is less than 5%. The rain drop size distribution (DSD) model used in the simulations was the normalized gamma distribution $n(D)$, as presented in many polarimetric radar rainfall studies (Testud et al. 2000; Bringi and Chandrasekar 2001; Illingworth and Blackman 2002):

$$n(D) = N_W f(\mu)\left(\frac{D}{D_0}\right)^{\mu} \exp\left[-(\mu + 3.67)\frac{D}{D_0}\right], \quad (1)$$

where $n(D)$ (m^{-3} mm^{-1}) is the volume density, D_0 (mm) is the median volume diameter, N_W (mm^{-1} m^{-3}) is the intercept parameter, and μ (no units) the shape parameter. The SCOP-ME rainfall rate relation is given by the following equation (Kalogiros et al. 2013a):

$$R = 0.8106 F_R(\mu) N_W D_0^{4.67} f_{R_2}(D_0), \quad (2)$$

where the factor $f_{R2}(D_0)$ accounts for an exponential relationship more accurate than the usual power law (Atlas et al. 1973; Bringi and Chandrasekar 2001) and for the terminal velocity of raindrops against their diameter. The median volume diameter D_0, the intercept parameter N_W, and the shape parameter μ of the DSD are estimated from the polarimetric radar measurements Z_H, Z_{DR}, and K_{DP} using the following equations. The function $F_R(\mu)$ is given by

$$F_R(\mu) = 0.6 \times 10^{-3} \pi \times 3.78 \frac{6}{3.67^4} \frac{(3.67 + \mu)^{\mu+4}}{\Gamma(\mu + 4)} \times \frac{\Gamma(\mu + 4.67)}{(\mu + 3.67)(\mu + 4.67)}, \quad (3)$$

where Γ indicates the gamma function. The DSD governing parameters (D_0 and N_W) are estimated from the following relationships:

$$D_0 = D_Z f_{D_0}(D_Z), \quad (4a)$$

$$D_Z = D_{Z_1} f_{D_{Z_1}}(D_{Z_1}),$$

$$D_{Z_1} = 0.1802 \left[\frac{Z_H}{K_{DP}} \xi_{DR}^{-0.2929}(1 - \xi_{DR}^{-0.4922})\right]^{1/3}, \quad (4b)$$

$$N_W = 3610 \left[\frac{K_{DP}}{(1 - \xi_{DR}^{-0.3893})}\right] D_0^{-4} f_{N_{W_2}}(D_Z), \quad (4c)$$

$$\mu = 165 e^{-2.56 D_0} - 1, \quad (4d)$$

where D_Z is the reflectivity-weighted mean diameter (mm), ξ_{DR} is the differential reflectivity in linear units (ratio of reflectivity at horizontal and vertical polarization), and the horizontal reflectivity Z_H in these relations is also given in linear units (mm^6 m^{-3}). The constraint of the shape parameter μ in Eq. (4d) was obtained from long-term disdrometer data, as described in Kalogiros et al. (2013a), with a method of best fit of the normalized gamma distribution to the measured DSD. The shape parameter was not estimated with a moments method like in Vivekanandan et al. (2004) because this involves estimation of high-order moments of the DSD (up to fifth- or sixth-order moment), which are characterized by large error due to the measurement errors in the high tail (high raindrop diameter values) of the DSD. The available disdrometer data supported the idea of a constrained gamma DSD and agree with Zhang et al. (2001) and Vivekanandan et al. (2004) for $D_0 < 2$ mm. The functions $f_p(D_Z)$, where the subscript

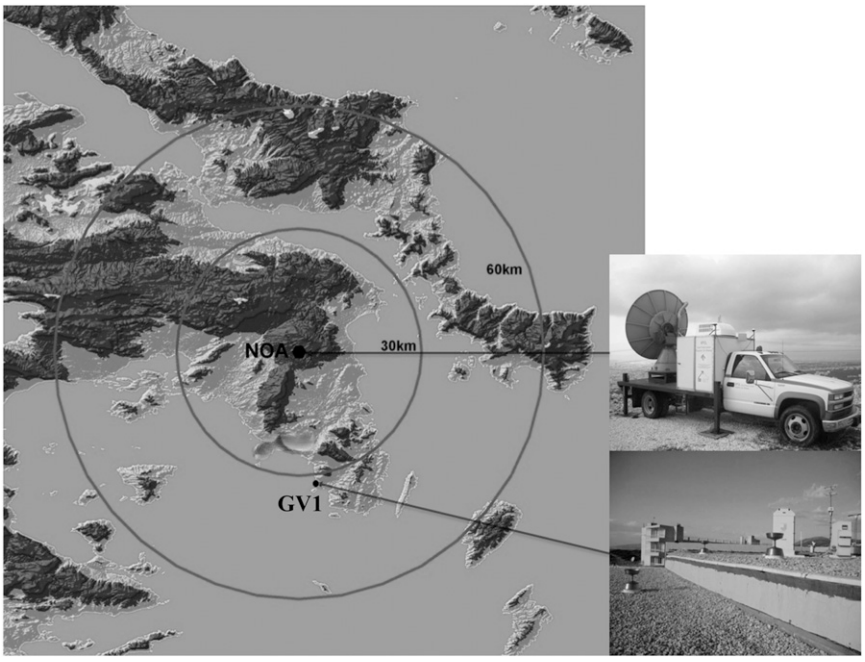

FIG. 1. Experimental area showing the radar site (NOA) and the in situ 2D video disdrometer site (GV1). On the right are pictures of the XPOL at NOA and the disdrometer at the GV1 site.

p indicates the corresponding parameter, are third-degree rational polynomial regression functions, which were found to adequately describe the Mie character of scattering and to include most of the dependence on D_Z:

$$f_p(D_Z) = \frac{\sum_{n=0}^{3} a_n D_Z^n}{\sum_{n=0}^{3} b_n D_Z^n}. \quad (5)$$

The coefficients of the polynomials in the numerator and denominator of $f_p(D_Z)$ are given in the appendix (Table A1) for the corresponding relations.

Before applying the microphysical retrieval algorithm (as well all the algorithms presented in this section and the following sections), reflectivities Z_H and Z_{DR} are corrected for the attenuation in rain. Path attenuation of a radar signal is significant, especially for high-frequency radars (like X band). For the correction of path attenuation in rain the SCOP algorithm is used. This algorithm is a self-consistent polarimetric algorithm, based on the parameterizations of the specific attenuation coefficients and backscattering phase shift in rain, derived by Kalogiros et al. (2013a), and applied with an iterative scheme to separate radar rays (Kalogiros et al. 2013b). As was shown by Kalogiros et al. (2013a), the parameterizations of the specific attenuation coefficients and backscattering phase shift are quite robust and independent of the constraining function of DSD shape parameter μ against D_0 [Eq. (4d)]. This independence is due to the use of D_Z in the parameterizations. Application to radar data and comparison with disdrometer data and other polarimetric algorithms presented in the literature (Testud et al. 2000; Gorgucci et al. 2006) showed that this algorithm performed similarly to or better than the other attenuation correction algorithms. However, all algorithms presented a systematic underestimation at high values of differential attenuation, probably due to the presence of hail in the path of the radar beam during those cases, which are not considered in these correction algorithms (Marzano et al. 2010).

In addition, various rainfall and rain microphysics algorithms available in the literature are evaluated in this work against the new polarimetric algorithm SCOP-ME. The ''standard'' reflectivity-to-rainfall relationship is the most widely used method in radar–rainfall estimation (hereafter called R–Z_H) as it relates directly to the radar reflectivity measured by any conventional weather radar:

$$R_{Z_H} = \alpha_1 Z_H^{\beta_1}. \quad (6)$$

The coefficients (i.e., α_1 and β_1) of this algorithm were determined from radar data collected during the years 2005–2006 in the area of Athens (Greece) by Kalogiros et al. (2006) and tested with various radar datasets by Anagnostou et al. (2009, 2010).

TABLE 1. Selected rain cases with corresponding statistical analysis for each event. The first column is the date of the event. The "Corr" column shows the value of the correlation between the reflectivity Z_H values measured by XPOL and the 2DVD for each event. The columns labeled "max," "mean," " % rain > 1 mm h^{-1}," and "% rain > 10 mm h^{-1}" the statistics of 2DVD (left-hand side of each column) and XPOL (right-hand side of each column).

Date	Corr	Max (mm h^{-1})		Mean (mm h^{-1})		% rain > 1 mm h^{-1}		% rain > 10 mm h^{-1}	
14 Jan 2008	0.88	81.4	130.3	11.7	12.7	31.8	34.9	10.6	10.6
28 Mar 2008	0.79	13.0	9.6	1.3	1.9	46.8	60.7	0.7	0.0
2 Apr 2008	0.8	34.0	33.8	5.7	4.6	87.2	83.5	14.9	8.8
5 Apr 2008	0.88	17.9	14.8	2.0	2.0	41.2	43.2	2.0	1.5
22 Sep 2008	0.63	2.5	2.1	1.3	1.3	73.3	66.7	0.0	0.0
25 Sep 2008	0.84	87.8	53.6	29.5	20.6	64.0	80.0	48.0	48.1
17 Nov 2008	0.68	11.7	8.7	2.4	2.0	35.2	34.6	0.6	0.0
29 Nov 2008	0.78	13.0	15.7	3.5	2.7	75.0	67.5	5.0	2.5
2 Jan 2009	0.78	4.7	7.9	0.8	0.9	17.6	24.2	0.0	0.0
5 Jan 2009	0.78	4.1	5.3	1.0	1.1	38.3	41.3	0.0	0.0
8 Jan 2009	0.64	14.3	9.4	3.8	2.7	31.0	31.0	3.5	0.0
13 Jan 2009	0.69	4.5	6.8	1.3	1.6	39.0	40.4	0.0	0.0
31 Jan 2009	0.51	5.1	37.5	1.8	6.5	66.7	88.1	0.0	15.1
8 Feb 2009	0.76	12.5	9.4	3.7	2.7	62.5	57.1	3.6	0.0
5 Mar 2009	0.81	11.0	10.3	2.8	2.5	84.6	83.5	1.2	1.1
12 Mar 2009	0.69	4.0	6.1	1.2	1.7	47.7	58.1	0.0	0.0
21 Mar 2009	0.63	16.0	37.5	4.0	5.7	75.5	77.4	4.7	1.4
5 Apr 2009	0.59	0.6	1.5	0.3	0.7	0.0	2.9	0.0	0.0
17 Oct 2009	0.76	2.1	2.0	0.7	0.9	16.9	27.7	0.0	0.0
25 Oct 2009	0.75	31.5	25.7	2.4	2.4	61.6	75.3	3.4	4.1
12 Nov 2010	0.82	29.5	53.2	4.2	8.7	12.5	17.6	4.2	8.0
16 Jan 2011	0.48	6.1	8.5	2.1	2.9	76.0	86.0	0.0	0.0
27 Jan 2011	0.59	7.8	7.8	2.1	2.2	70.6	66.7	0.0	0.0
2 Feb 2011	0.57	3.0	11.1	0.7	2.6	09.4	24.3	0.0	0.7
18 Feb 2011	0.54	3.8	7.5	1.0	1.5	14.9	16.6	0.0	0.0
20 Feb 2011	0.52	14.7	16.8	1.1	1.8	16.9	29.2	1.5	3.1
2 Mar 2011	0.78	5.3	5.3	1.3	1.3	54.8	59.6	0.0	0.0
29 Mar 2011	0.56	3.9	3.9	1.0	1.5	34.1	59.7	0.0	0.0

The differential phase shift–rainfall relationship (hereafter called R–K_{DP}), for X-band radars is, on average, nearly linearly related to the rainfall rate:

$$R_{K_{DP}} = \alpha_2 K_{DP}^{\beta_2}. \quad (7)$$

Various researchers have adopted formulations, which are special cases of the following power-law expression (hereafter named "combined" or R–$Z_H Z_{DR} K_{DP}$):

$$R_{Z_H Z_{DR} K_{DP}} = a Z_H^b Z_{DR}^c K_{DP}^d. \quad (8)$$

The coefficients α_1, α_2, β_1, β_2, a, b, c, and d are given in the appendix (Table A2) and are obtained by performing a multiple regression of Eqs. (6)–(8) using T-matrix simulations as in Kalogiros et al. (2006), Montopoli et al. (2008b), and Marzano et al. (2010).

3. Results

The performances of the SCOP-ME rain microphysics algorithm and other algorithms, described in section 2, are evaluated using measurements from the National Observatory of Athens (NOA) high-resolution dual-polarization Doppler X-band radar (XPOL) during the period from 2008 to 2011 in the urban area of Athens. XPOL is one of the first mobile research-quality radars, which have been extensively used since 2000 in different scientific field experiments in the United States, Greece, and Italy (E. N. Anagnostou et al. 2004, 2006; M. N. Anagnostou et al. 2006, 2009, 2010). XPOL was deployed at the NOA premises 500 m MSL. The radar conducted plan position indicator (PPI) scans at three different antenna elevations (0.5°, 1.0°, and 1.5°) over an azimuth sector scan of 120°–330° with 150-m range resolution for a total range of 60 km. Antenna rotation rate was 6° s^{-1} and the total time for a volume scan was about 3 min. An optical 2D video disdrometer (2DVD) was deployed within a 35-km range at a coastal area southeast of the XPOL site (see Fig. 1), providing high temporal-resolution (1 min) drop size distribution measurements. There were no terrain obstacles in the path from the radar to the disdrometer.

Twenty-one rain events of coincident XPOL and disdrometer observations with significant rain in the

path between the radar and the disdrometer were selected from the database (see Table 1). The selection of the cases was based on the quality control of the radar and the 2DVD observations. To limit the effects of sampling differences and the separation in altitude between the disdrometer and the radar volume, only rain events with correlation greater than 0.5 between the disdrometer-derived and radar-observed reflectivity were selected. Furthermore, only the lower radar elevations (below 1°) were used in order to avoid possible melting layer effects during some stratiform rain events. The bias calibration of Z_H and Z_{DR} is made using long-term disdrometer data, as described in Kalogiros et al. (2013b). Furthermore, the calibration of Z_{DR} is also improved using a real-time method, which is based on an average Z_H–Z_{DR} relation. The effect of calibration biases and random noise on the SCOP-ME microphysics and rain algorithms was examined using simulations (Kalogiros et al. 2013a). For the above typical values of errors, it was found that the proposed algorithms are accurate within 20%. We note that without bias and random errors the accuracy of the algorithms is better than 5%, as mentioned in section 2. However, a point to mention is that the measurement errors contribute mainly to the random part of the error, assuming that bias calibration has been made with a typical accuracy of ~1 dBZ for Z_H and ~0.2 dB for Z_{DR}.

A rain classification procedure, similar to that of Montopoli et al. (2008b), was adopted to separate the stratiform from convective rain types in the disdrometer time series. The classification procedure is based on the criterion that stratiform rain tends to be horizontally uniform and low in intensity as opposed to the convective regime, which generally shows high intensities at short time periods. Following the procedure discussed by Montopoli et al. (2008b), the DSD features were compared in terms of the mass-weighted mean diameter $D_M = D_0\,(\mu + 4)/(\mu + 3.67)$ for a normalized gamma DSD as a function of $\log_{10}N_W$. Figure 2 indicates a classification separation between the stratiform and convective rain types using a linear least squares fit applied to the values of D_M and $\log_{10}N_W$ from the 2DVD DSD observations, which agrees with the relationship from Montopoli et al. (2008b). The linear least squares fit applied to all coincident 2DVD with XPOL values of D_M and $\log_{10}N_W$, as $\log_{10}N_W = p_1D_M + p_2$ for both the stratiform and convective rain types. The values of the p_1 and p_2 are taken from Montopoli et al. (2008b), as shown in Table 2. Note that, according to Table 1, there are six convective type events of maximum rainfall rate >30 mm h^{-1} out of the 21 selected cases.

The statistical metrics for the evaluation of the algorithms include: 1) the relative mean error (rME), which is defined as the mean of the error (i.e., difference between reference values and radar estimates), normalized by the mean of the reference values; 2) the relative rms error (rRMSE), normalized by the storm average derived from the reference values; and 3) the efficiency score (Eff), described by Nash and Sutcliffe (1970), defined as the difference between unity and the ratio of the error variance to reference variance. Eff is a statistical measure of the variability of the error normalized by the natural variability of the estimated parameter and is scaled from $-\infty$ to 1. A value of one indicates that the estimate is perfect. An efficiency value equal to 0 or negative indicates that the estimation is, respectively, no better or even worse than using simply the mean value of the predicted parameter.

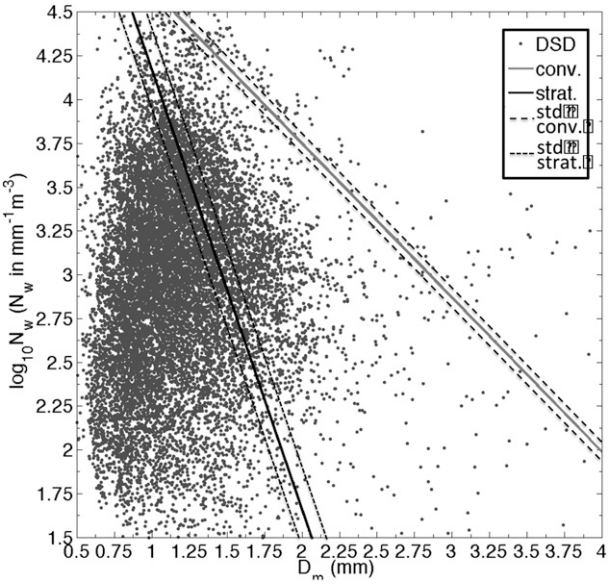

FIG. 2. Scatterplot of the mean diameter (D_m) vs the intercept parameter $\log_{10}$ (N_W). The two least squares fits (taken from Montopoli et al. 2008b) of the data points are shown for the stratiform (left, black solid line) and convective (right, gray solid line) cluster.

Statistical error analysis of Z_H and Z_{DR}, observed by XPOL and corrected for attenuation, is performed for different values of path-integrated attenuation (PIA) equal to 0.5–2, 2–4, 4–6, and >6 dB. PIA was determined by calculating the difference of the measured reflectivity by XPOL to the reflectivity calculated from disdrometer measurements using the T-matrix algorithm

TABLE 2. Coefficient for the D_M, $\log_{10}N_W$ linear relationship.

Cluster type	p_1	p_2
Stratiform	−2.51	6.68
Convective	−0.88	5.51

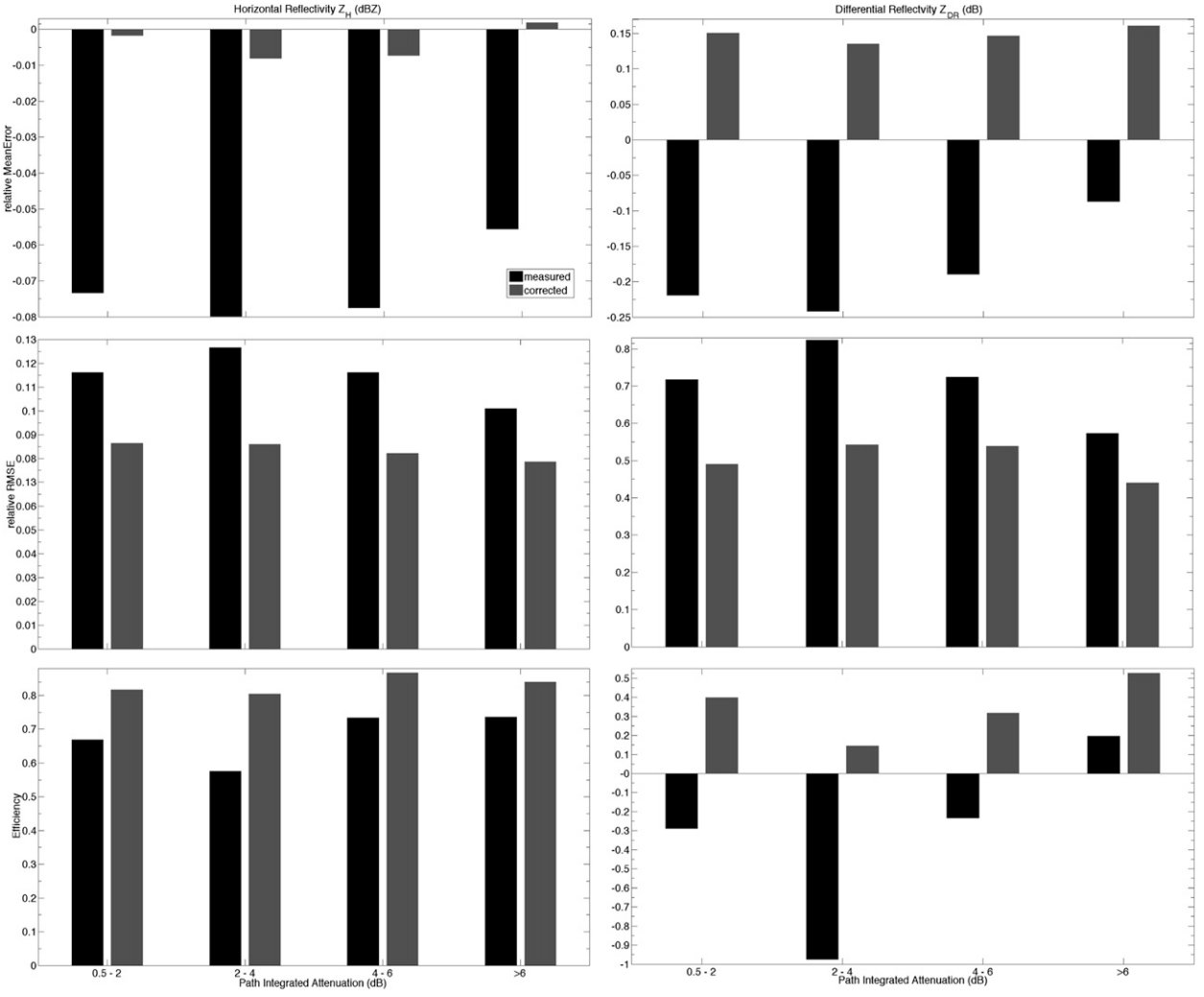

FIG. 3. Bulk error statistics (rME, rRMSE, and Eff) of radar observed and corrected for specific attenuation (left) horizontal polarization reflectivity and (right) differential reflectivity vs the path-integrated attenuation (PIA).

(Mishchenko 2000). The analysis was performed for the lowest two radar elevations (0.5° and 1.0°) and for Z_H and Z_{DR} greater than 10 dBZ and 0.5 dB, respectively. Figure 3 shows that the attenuation-corrected Z_H measurements have low rME (almost 1%) and rRMSE (around 10%–13%) for all PIA categories. The efficiency score is also high (>0.8) for values of PIA even higher than 6 dB. The point to note is that the performance of the attenuation correction algorithm is nearly independent of the PIA. Evaluation for Z_{DR} shows slightly worse results at PIA values below 6 dB, which implies low intensity rainfall rates, exhibit overestimation of about 15% and the relative RMSE in the range from 60% to 85%. However, as shown by Kalogiros et al. (2013b), in the cases of strong convective cells with large PIAs (>6 dB) and observed Z_{DR} less than −1 dB, the SCOP correction method was found to systematically underestimate, probably because of the presence of mixed-phase hydrometeors (hail in addition to rain) in the path of the radar beam.

a. Rainfall rate error statistics

The bulk statistics are performed as a function of the four different PIA ranges (i.e., 0.5–2, 2–4, 4–6, and >6 dB) and for values of reference rainfall rates greater than 0.1 mm h^{-1}. The rainfall error statistics are performed for the three above-mentioned rainfall estimation algorithms (i.e., R–Z_H, R–K_{DP}, and R–$Z_H Z_{DR} K_{DP}$) and SCOP-ME. For evaluation of the rainfall algorithms, in addition to the rME, rRMSE, and Eff, we also used the Heidke skill score (HSS), which measures the correspondence between the estimate and the reference

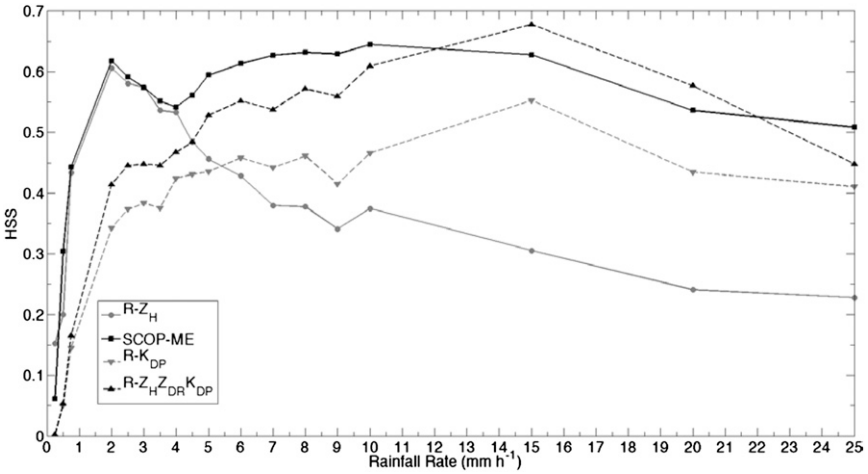

FIG. 4. One-dimensional HSS plot vs rainfall rate (mm h^{-1}) threshold.

(Barnston 1992; Conner and Petty 1998). The one-dimensional (1D) plot of HSS values at different rainfall rate thresholds is presented in Fig. 4. The SCOP-ME has a higher HSS compared to R–Z_H and R–K_{DP} and a similar HSS compared to the R–$Z_H Z_{DR} K_{DP}$ algorithm at low rainfall rates (<4 mm h^{-1}), which contribute 94% of the cumulated rainfall. For medium to high rainfall rates (5–12 mm h^{-1}), SCOP-ME exhibits better performance compared to the other three retrieval methods.

Table 3 summarizes the bulk statistics of the algorithm estimates for different time integrations (15, 30, and 60) in rainfall (in millimeters). It is evident from the table that the two algorithms with the lowest rME (range from 0.03 to 0.04 and −0.17 to −0.16), rRMSE (range from 0.51 to 0.63 and 0.60 to 0.69), and Eff (range from 0.79 to 0.83 and 0.73 to 0.87) are the SCOP-ME and R–$Z_H Z_{DR} K_{DP}$ algorithms, respectively. The quite good statistics of the SCOP-ME rainfall algorithm [Eq. (2)], despite the significant error of N_W (as shown in section 3b below), is due to the dependence on the power of D_0. As shown in the section, the efficiency for the estimation of D_0 is significantly better than N_w. Thus, N_w is, on average, only estimated correctly from the algorithms (SCOP-ME performs better than the other algorithms examined in this work), and rainfall rate estimate variations are mainly due to D_0 variations. Overall, SCOP-ME outperforms all three algorithms in terms of the examined error statistics, having from 3 to 12 times less rME and higher Eff (10%–21%) scores.

Figure 5 presents the error metrics for the three different rainfall estimation algorithms and SCOP-ME versus PIA. Similar to Fig. 3, the SCOP-ME algorithm has very low rME (ranging between 1% and 5% in absolute values) and is nearly insensitive to PIA. It also has the largest Eff (0.82–0.73) and the smallest rRMSE (0.8–0.65) values. On the other hand, the R–Z_H rainfall algorithm suffers from large errors at high PIAs, while the combined method R–$Z_H Z_{DR} K_{DP}$ performs better when compared to the other two methods. A point to note is that the rME of the combined method exhibits a slight increase (~2% in absolute values) with respect to PIA. Dependency on PIA indicates that the combined algorithm is more sensitive to the attenuation correction errors.

b. Rain microphysics error statistics

This section investigates the accuracy of the estimation of DSD-normalized gamma model parameters from XPOL observations. The SCOP-ME algorithm error statistics are compared against two algorithms from the literature, the Park et al. (2005, hereafter P05) and Gorgucci et al. (2008, hereafter G08). Error statistics were evaluated, as in previous sections, through comparison against the 2DVD DSD observations. Figure 6 shows scatterplots of the XPOL estimates of two DSD parameters (N_w and D_0) against parameters derived from 2DVD observations using the DSD moments method (Bringi et al. 2003). The x axis indicates the

TABLE 3. Total bulk statistics in terms of rainfall (mm) for the four different radar rainfall estimation algorithms compared with 2DVD DSD observations as a function of time integrations (15, 30, and 60 min).

	15/30/60 (min)		
	rME	rRMSE	Eff
SCOP-ME	0.04/0.03/0.04	0.63/0.59/0.51	0.82/0.79/0.83
R–Z_H	−0.21/−0.21/−0.18	0.81/0.77/0.74	0.70/0.65/0.64
R–K_{DP}	−0.37/−0.37/−0.37	0.72/0.73/0.69	0.76/0.69/0.69
R–$Z_H Z_{DR} K_{DP}$	−0.16/−0.17/−0.16	0.69/0.68/0.60	0.78/0.73/0.76

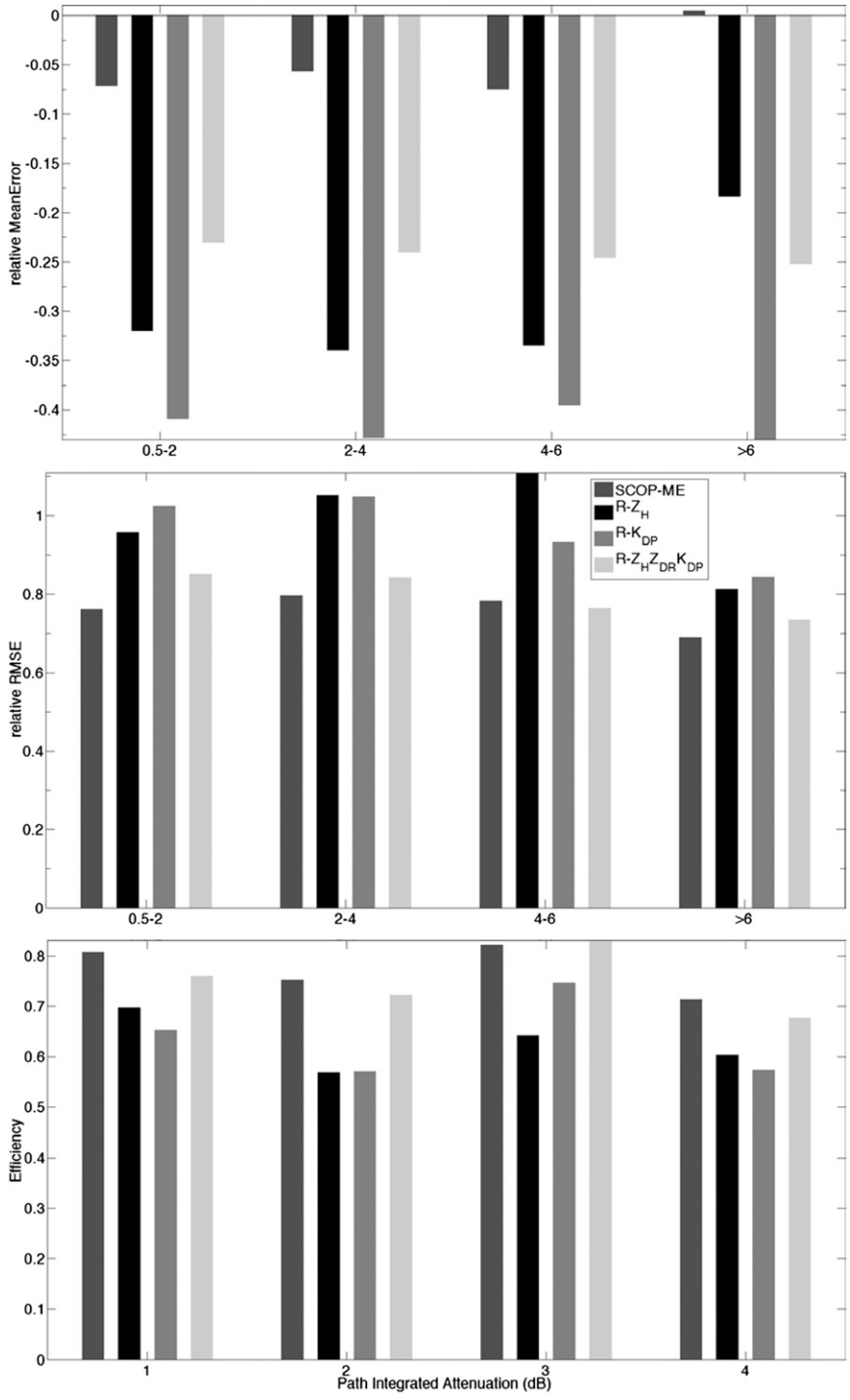

FIG. 5. Bulk error statistics (rME, rRMSE, and Eff) of the four radar rainfall algorithms vs PIA.

reference disdrometer observations, while the *y* axis shows the radar estimates. The top two panels are the radar estimates from the SCOP-ME algorithm, the middle one is of the G08 estimates, and the lower one of the P05 estimates. The scatterplot shows similar variability in all algorithms, which is probably due to the measurement error effects and radar volume versus point (disdrometer) measurement-scale mismatch and spatial separation. However, the bulk statistics evaluated on the above data (see Table 4) shows a very low rME for the SCOP-ME

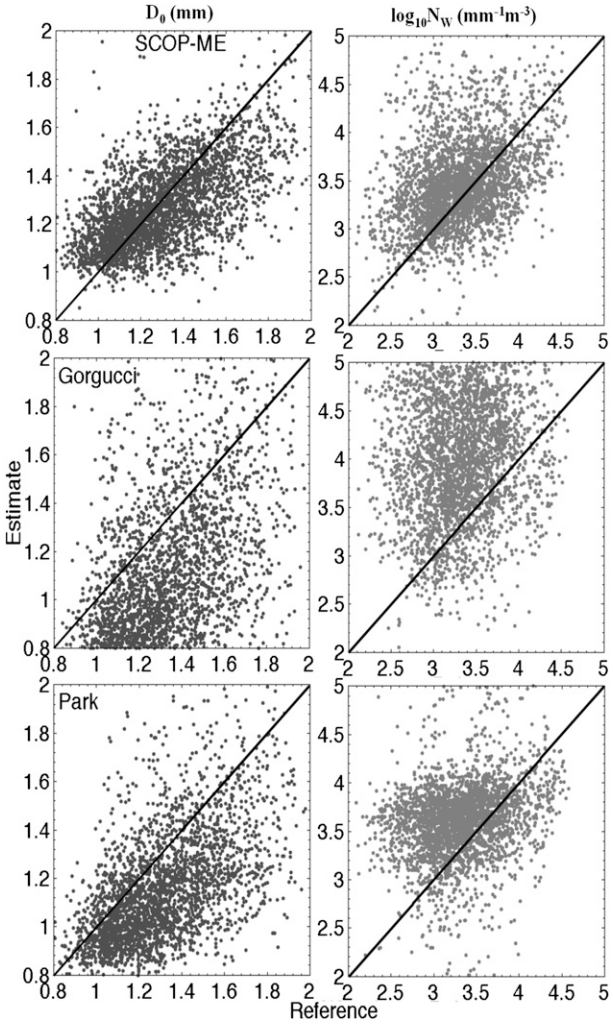

FIG. 6. Scatterplots of radar estimated (SCOP-ME, Park, and Gorgucci) D_0 and $\log_{10}N_W$ vs calculated from 2DVD observed spectra.

algorithm (-0.03 and 0.04) and notably higher efficiency scores (0.37 and -0.17) for both D_0 and N_W estimates when compared to the P05 and G08 algorithms. The efficiency is slightly negative for SCOP-ME, but it is worse for the other algorithms. This results show that the N_W estimate, by all algorithms, is significantly affected by noise or any other factors that contribute to data. Still, SCOP-ME is better than the other algorithms.

Figure 7 presents the joint frequency plots of the two DSD parameters ($\log_{10}N_W$ versus D_0). We note similarities in terms of size dimensions (on both the estimate and reference, the D_0 ranges between 1.1 and 1.8 and $\log_{10}N_W$ between 2 and 4) and the average slope of $\log_{10}Nw$–D_0 relation in the radar retrievals and the reference parameters. As shown in this figure, the core of the SCOP-ME density is more frequent than the reference, but it exhibits a lower error bias with respect to reference measurements. The G08 estimates give a slope similar to the slope of the reference measurements, but with significant bias. As shown in Fig. 6, this is due to the combination of D_0 underestimation and $\log_{10}N_w$ overestimation in the G08 estimates.

Figure 8 presents the bulk statistics of the error of the DSD parameters estimated from radar against the parameters derived from the 2DVD spectra observations (for Z_H values > 20 dBZ, $D_0 > 0.5$ mm, and $\log_{10}N_W > 1$ mm^{-1} m^{-3}) versus PIA. The SCOP-ME estimates exhibit the lowest rME (-0.5%–2% for D_0 and 1%–3% for $\log_{10}N_W$) and are insensitive to PIA. Similarly, rRMSE ranges from 11.7% to 12.7% for D_0 and 11.5% to 12.5% for $\log_{10}N_W$ and weakly depend on PIA. On the other hand, the other two methods exhibit moderate dependence on PIA, especially in the case of to the $\log_{10}N_W$ estimates. Specifically, the Eff score of $\log_{10}N_W$ estimation is below zero, indicating weakness of the ability of these algorithms to capture the variability of the parameter. In the case of rME, a point to note is that both P05 and G08 methods systematically underestimate D_0 and overestimate $\log_{10}N_W$ (see Fig. 6). The rRMSE of D_0 estimates ranges from 16% to 17% for the G08 and is around 14% for the P05. A significant dependence of the G08 D_0 estimate on PIA is noted. Similar results are observed in Table 4 for the $\log_{10}N_W$ estimates since the SCOP-ME method has small rME (equal to 0.04) and rRMSE (equal to 0.14). The P05 method shows results (0.09 for rME and 0.15 for rRMSE) similar to the SCOP-ME, whereas the G08 method systematically tends to overestimate (rME equal 0.24) with the rRMSE close to 0.19. The SCOP-ME method also exhibits a better Eff (equal to -0.17) when compared to the other two methods, the G08 and the P05 methods having a large negative Eff values equal to -1.15 and -0.31, respectively.

TABLE 4. Bulk statistics of the selected rain events for the three different radar rain microphysics estimation algorithms compared with 2DVD observations.

	P05/G08/SCOP-ME		
	rME	rRMSE	Eff
D_0 (mm)	$-0.12/-0.16/-0.03$	0.16/0.19/0.14	$0.13/-0.31/0.37$
$\log_{10}N_W$ (mm^{-1} m^{-3})	0.09/0.24/0.04	0.15/0.19/0.14	$-0.31/-1.15/-0.17$

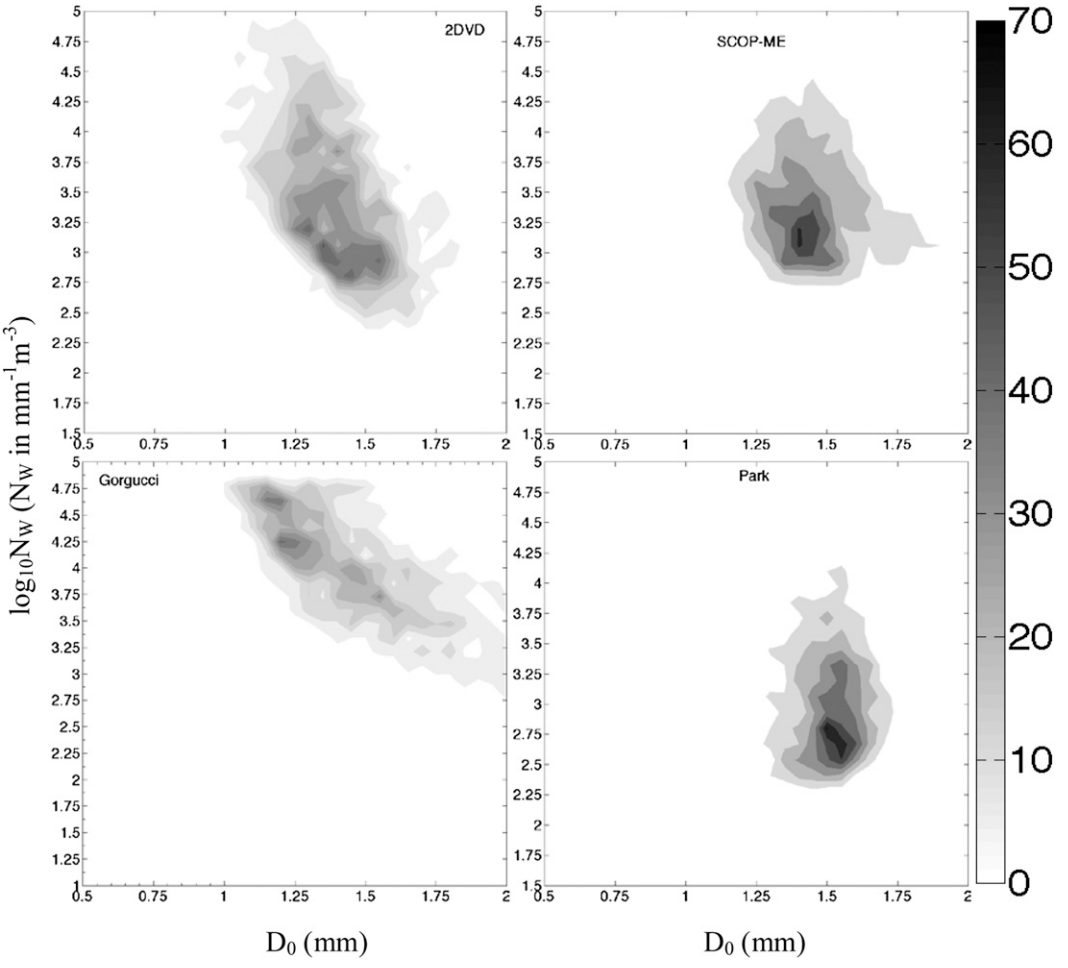

FIG. 7. Two-dimensional frequency contour plots of $\log_{10}N_W$ (mm^{-1} m^{-3}) vs D_0 (mm).

In summary, the critical issue in the improvement of polarimetric microphysical algorithms is the systematic error (bias) introduced by the model parameterization. This bias error is added to the total error and the discrepancy because of volume-to-point measurement-scale differences. Even though averaging could reduce the random measurement error, it cannot reduce the parameterization (bias) error. The minimization of the parameterization error is significant, as it was shown in Kalogiros et al. (2013a) by comparing simulations with measurement noise to disdrometer data. This is also proved in the current paper using radar data (e.g., Figs. 6, 7) compared to the other algorithms.

4. Case study analysis

In this section, evaluation of the rain algorithms is performed qualitatively with a visual interpretation of case studies, which include time series of selected rain events and total rain accumulation maps. The presented rain events are the 28 March 2008 event, which is a stratiform type rain event, and the 14 January 2008 event, which is a short-duration convective-type event. These events are used to compare the spatial differences of the four radar rainfall algorithms and the two microphysical estimation algorithms and their temporal covariance with corresponding rain microphysics observations from the 2DVD data.

Figures 9a and 9b present time series (with 15-min temporal resolution) of radar rainfall rate (mm h^{-1}) and DSD parameter (D_0 and $\log_{10}N_W$) estimates and disdrometer observations for the two rain events. The first case (stratiform event) evolves in two phases. The duration of the first phase is about 2 h, with its peak of about 5 mm h^{-1} at 0800 UTC. The second phase of the event started in the afternoon (1500 UTC) of the same date and dissipated just before midnight. In the second phase there are three rainfall peaks, each one of about 3 mm h^{-1}. Figure 9 shows that the SCOP-ME algorithm follows well the variations of the

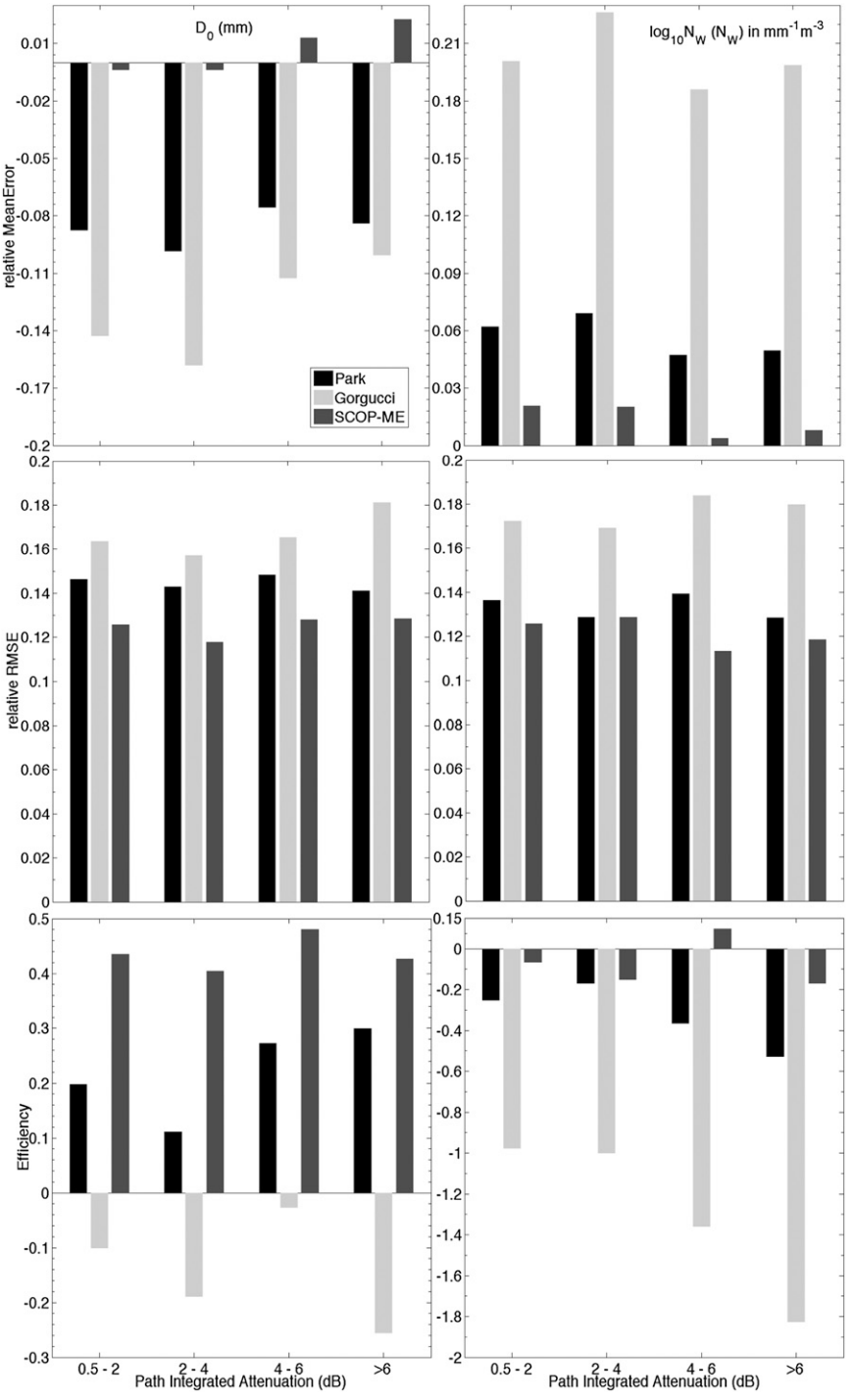

FIG. 8. Bulk statistics (rME, rRMSE, and Eff) of radar-estimated $\log_{10}N_W$ (mm^{-1} m^{-3}) and D_0 (mm) parameters vs PIA (dB).

disdrometer observations when compared to the other algorithms.

In the convective rain event a short-duration rainfall rate peak of ~35 mm h^{-1} is observed at midday. During the peak rainfall the SCOP-ME and the combined algorithm are the two algorithms that perform better. The SCOP-ME and the combined methods are the two algorithms with the best bulk statistics (0.13 and 0.07 for rME, 0.34 and 0.22 for rRMSE, and 0.98 and 0.99 for Eff) for the rainfall rate estimate. Regarding the DSD

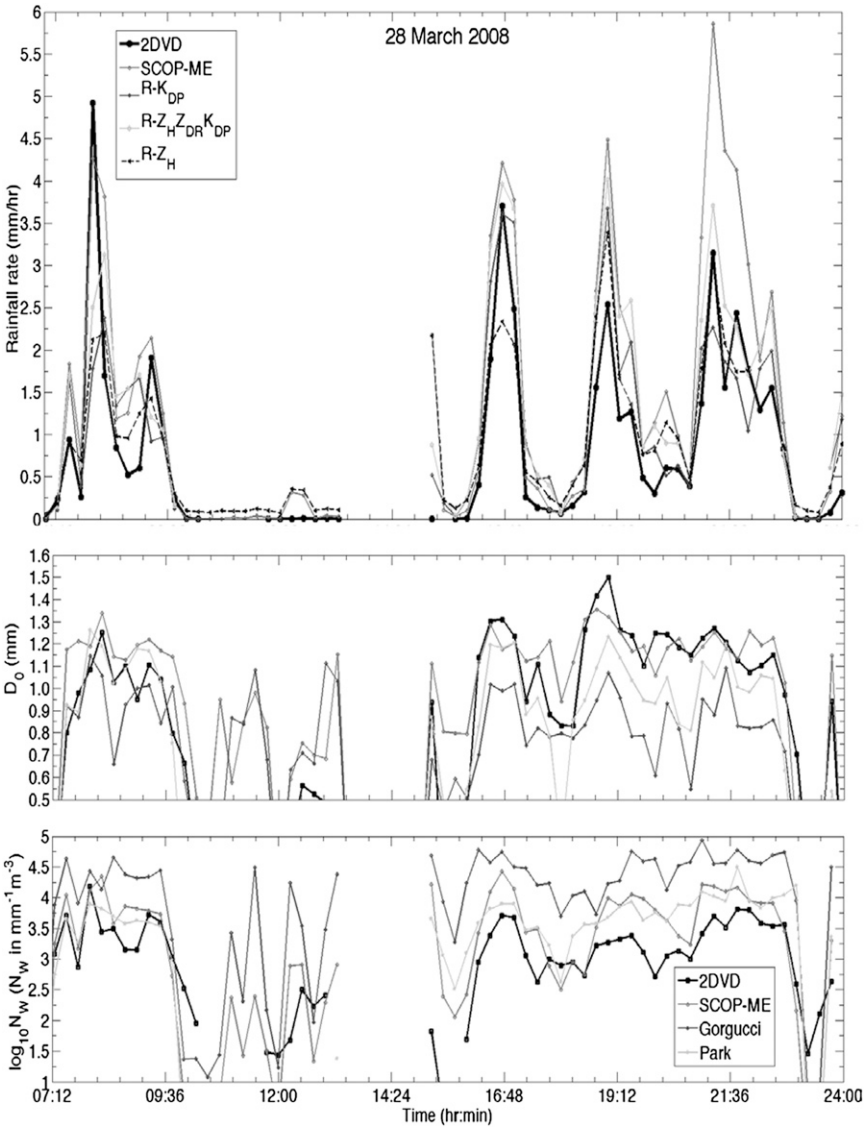

FIG. 9a. Time series of the 28 Mar 2008 rain event: (top) rainfall rates from the four radar rainfall algorithms and the 2DVD rainfall rate observations and DSD parameters, (middle) D_0 and (bottom) $\log_{10}N_W$, from the three different microphysical algorithms and the parameters calculated from the 2DVD measured spectra.

parameter estimation, the SCOP-ME shows a performance comparable with the G08 method in terms of rME for the D_0 parameter estimation (0.05 and −0.02, respectively), whereas for the $\log_{10}N_W$ parameter retrieval, SCOPE-ME shows the best performance. Furthermore, SCOP-ME shows better performances in terms of rRMSE (15% and 23%) and Eff scores (0.60 and −0.04) for D_0 and $\log_{10}N_W$ DSD parameter estimates, respectively.

5. Conclusions

The performance of a new combined self-consistent with optimal parameterization attenuation correction and rain microphysics estimation (SCOP-ME) algorithm for polarimetric X-band radars was investigated in this study. The proposed method performance was compared against three other radar rainfall algorithms (R–Z_H, R–K_{DP}, and R–$Z_H Z_{DR} K_{DP}$) and two DSD retrieval algorithms [Park et al. (P05) and Gorgucci et al. (G08)] derived from the literature. The evaluation included data collected during a 3-yr period (2008–11) with an X-band dual-polarization Doppler weather radar and coincident DSD observations from a 2D video disdrometer (35-km range from the radar) in the urban area of Athens, Greece.

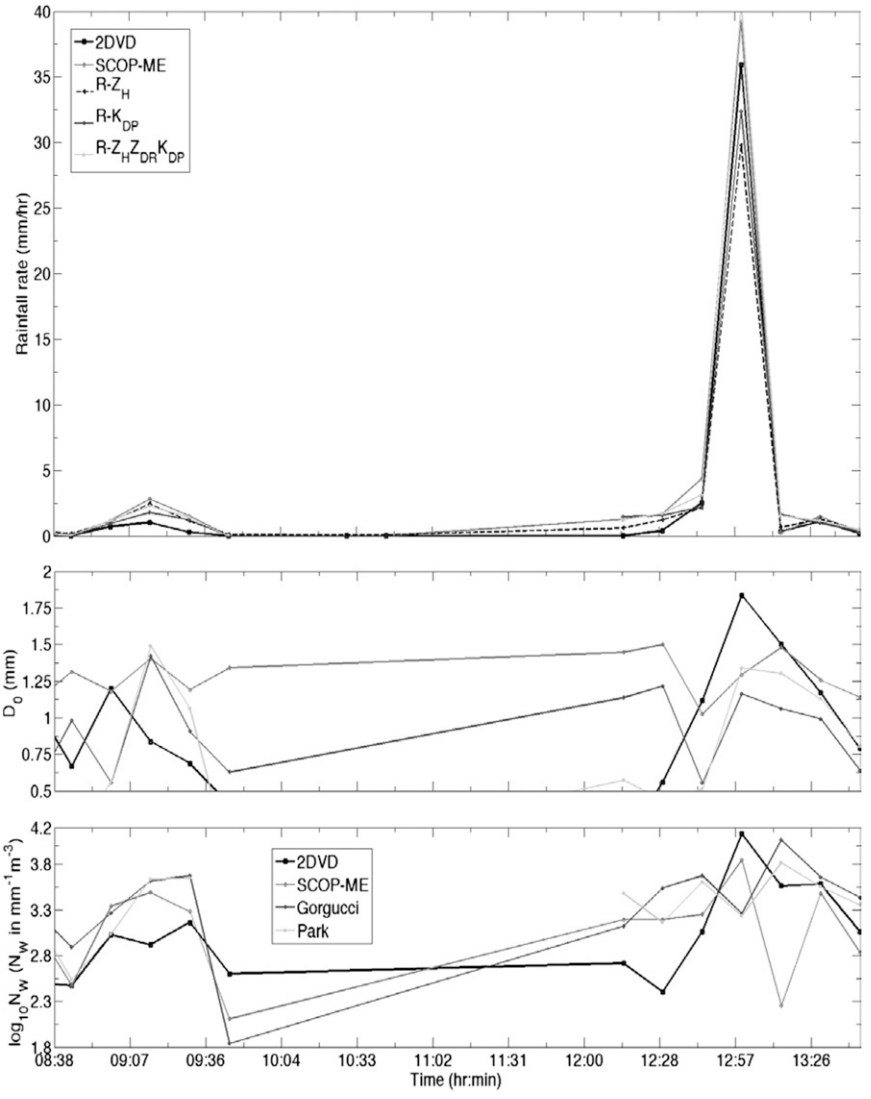

FIG. 9b. As in Fig. 9a, but for the 14 Jan 2008 rain event.

The SCOP-ME polarimetric rainfall and microphysics algorithm was developed from T-matrix simulations at X band, based on the Rayleigh scattering limit relations, with the addition of a rational polynomial dependence on reflectivity-weighted droplet diameter D_Z due to Mie scattering effects. The algorithm is based on the consideration that a gamma distribution model can adequately describe the shape of raindrop size distribution. For the evaluation of the SCOP-ME algorithm, a statistical error analysis of the horizontal polarization Z_H and differential Z_{DR} reflectivity observed with the radar and corrected for attenuation in rain against the corresponding radar products calculated from the 2DVD-observed DSD was performed as a function of different path-integrated attenuation values in four different categories (0.5–2, 2–4, 4–6, and >6 dB). The corrected-for-rain attenuation Z_H and Z_{DR} overall showed very good performance with low relative error compared to the measured ones. We have shown that the correction of Z_H is nearly independent of PIA.

Error statistics of the three rainfall estimation algorithms and the SCOP-ME algorithm, evaluated against the disdrometer rainfall observations, showed that the SCOP-ME has a low relative error in all PIA categories compared to the other three methods, while the other algorithms systematically underestimate rainfall. The efficiency statistics, determined from SCOP-ME estimates, exhibited better results at low to moderate (0.5–4 dB) PIAs and comparable results at large (>4 dB) PIAs to the combined R–$Z_H Z_{\mathrm{DR}} K_{\mathrm{DP}}$ rainfall algorithm. The Heidke skill score statistic had comparable results

of the SCOP-ME, with the R–$Z_H Z_{DR} K_{DP}$ rainfall algorithm at low rainfall rates (<4 mm h^{-1}), while for moderate to high rainfall rates (4–12 mm h^{-1}) SCOP-ME exhibited better results.

The SCOP-ME rain microphysics algorithm was also compared to two existing DSD parameter estimation algorithms. Overall, SCOP-ME was shown to have lower relative error statistics when compared to the other algorithms. The SCOP-ME algorithm performed better for all PIA ranges and rainfall rates and provided relatively accurate retrievals of the DSD parameters. However, the estimation of N_w by all algorithms is significantly affected by noise or other factors like radar volume versus point (disdrometer) measurement-scale mismatch and spatial separation. Thus, N_w is, on average, only estimated correctly from all algorithms. The good statistics for rainfall rate estimate with SCOP-ME are due mainly to D_0 variation, which is usually estimated much more effectively than N_w.

Although the study included a long-term dataset, the latter is still to be considered limited in terms of hydroclimatic regime variability. Additional studies based on data from different climatic regions (i.e., tropical, oceanic, complex terrain, etc.) and more extensive ground validation observations are needed to verify the extended performance and also the generalization capability of the SCOP-ME retrieval technique for different storm types and radar ranges. Furthermore, future work should focus on precipitation classification (snow, hail, graupel, in addition to rain) and development of radar microphysics algorithms for each precipitation type. Neural networks and fuzzy logic are tools to be considered in future extensions of this work.

Acknowledgments. This work is part of the HYDRORAD project (research for the benefit of SMEs category, Grand Agreement FP7-SME-2008-1-232156) funded by the EC Seventh Framework Programme from 2009 until 2011. Marios N. Anagnostou thanks the support of the Marie Curie Fellowship under Grant Agreement 236871 HYDREX, coordinated by the Sapienza University of Rome, Italy, and the support of the Postdoctoral Fellowship by the Greek General Secretariat for Research and Technology under Grant Agreement PE10(975) HYDRO-X, coordinated by the National Observatory of Athens, Greece, in the framework of the program ''Education and Lifelong Learning'' funded by Greece and the EU European Social Fund.

APPENDIX

Fitted Coefficients of the Rational Polynomial

The values of the coefficients of the rational polynomial functions of Eq. (5) in the parameterization of rainfall rate by Eqs. (2)–(4) at X band (9.37 GHz) are reported in Table A1, and fitted coefficients of Eqs. (6)–(8) from the simulated spectra DSD in Table A2. It is worth noting that the simulated radar observables for the regression analysis, used to estimate the coefficients of Eqs. (7) and (8) in Montopoli et al. (2008a), are DSD spectra taken from seven different climatological regions (i.e., three from Japan, two from the United States, one from the United Kingdom, and one from Greece). Moreover, in the simulated radar observables, three different types of noise due to instrumental, reconstruction, and attenuation correction errors are included.

TABLE A1. Values of the coefficients of the rational polynomial functions Eq. (5) in the parameterization of rainfall rate by Eqs. (2)–(4) at X band (9.37 GHz).

Function	a_0/b_0	a_1/b_1	a_2/b_2	a_3/b_3
f_{D0} in Eq. (4a)	0.9542/1.0000	0.2989/0.2243	0.0577/0.2949	0.0030/−0.005
f_{Dz1} in Eq. (4b)	0.9190/1.0000	0.1501/−0.2248	−0.1722/0.0182	0.0511/0.023
f_{Nw2} in Eq. (4c)	1.0000/1.0000	−0.6792/−0.6410	0.2112/0.1551	−0.0109/−0.006
f_{R2} in Eq. (4d)	1.0000/1.0000	−1.2313/−0.2176	2.1166/0.3064	0.6842/1.230

TABLE A2. Fitted coefficients of Eqs. (6)–(8) from the simulated spectra DSD.

α_1	β_1	α_2	β_2	a	B	C	d
3.36×10^{-2}	0.58	11.37	0.98	1.88	0.25	−1.07	0.61

REFERENCES

Anagnostou, E. N., and W. F. Krajewski, 1999: Real-time radar rainfall estimation. Part I: Algorithm formulation. *J. Atmos. Oceanic Technol.,* **16,** 189–197.

——, M. N. Anagnostou, W. F. Krajewski, A. Kruger, and B. J. Miriovsky, 2004: High-resolution rainfall estimation from X-band polarimetric radar measurements. *J. Hydrometeor.,* **5,** 110–128.

——, M. Grecu, and M. N. Anagnostou, 2006: X-band polarimetric radar rainfall measurements in Keys Area Microphysics Project. *J. Atmos. Sci.,* **63,** 187–203.

Anagnostou, M. N., E. N. Anagnostou, and J. Vivekananda, 2006: Correction for rain-path specific and differential attenuation of X-band dual-polarization observations. *IEEE Trans. Geosci. Remote Sens.,* **44,** 2470–2480.

——, ——, and J. Vivekanandan, 2007: Comparison of raindrop size distribution estimates from X-band and S-band polarimetric observations. *IEEE Geosci. Remote Sens. Lett.,* **4,** 601–605.

——, ——, G. Vulpiani, M. Montopoli, F. S. Marzano, and J. Vivekanandan, 2008: Evaluation of X-band polarimetric radar estimates of drop size distributions from coincident S-band polarimetric estimates and measured raindrop spectra. *IEEE Trans. Geosci. Remote Sens.,* **46,** 3067–3075.

——, J. Kalogiros, E. N. Anagnostou, and A. Papadopoulos, 2009: Experimental results on rainfall estimation in complex terrain with a mobile X-band polarimetric weather radar. *Atmos. Res.,* **94,** 579–595.

——, ——, ——, M. Tarolli, A. Papadopoulos, and M. Borga, 2010: Performance evaluation of high-resolution rainfall estimation by X-band dual-polarization radar for flash flood applications in mountainous basins. *J. Hydrol.,* **394,** 4–16.

Atlas, D., and C. W. Ulbrich, 1990: Early foundations of the measurement of rainfall by radar. *Radar in Meteorology,* D. Atlas, Ed., Amer. Meteor. Soc., 86–97.

——, R. C. Srivastava, and R. S. Sekron, 1973: Doppler radar characteristics of precipitation at vertical incidence. *Rev. Geophys.,* **11,** 1–35.

Barnston, A. G., 1992: Correspondence among the correlation, RMSE, and Heidke forecast verification measures: Refinement of the Heidke score. *Wea. Forecasting,* **7,** 699–709.

Battan, L. J., 1973: *Radar Observations of the Atmosphere*. University of Chicago Press, 323 pp.

Beard, K. V., and C. Chuang, 1987: A new model for the equilibrium shape of raindrops. *J. Atmos. Sci.,* **44,** 1509–1524.

Bringi, V. N., and V. Chandrasekar, 2001: *Polarimetric Doppler Weather Radar*. Cambridge University Press, 662 pp.

——, ——, J. Hubbert, E. Gorgucci, W. L. Randeu, and M. Schoenhuber, 2003: Raindrop size distribution in different climatic regimes from disdrometer and dual-polarized radar analysis. *J. Atmos. Sci.,* **60,** 354–365.

Conner, M. D., and G. W. Petty, 1998: Validation and intercomparison of SSM/I rain-rate retrieval methods over the continental Unites States. *J. Appl. Meteor.,* **37,** 679–700.

Gorgucci, E., G. Scarchilli, V. Chandrasekar, and V. N. Bringi, 2001: Rainfall estimation from polarimetric radar measurements: Composite algorithms immune to variability in raindrop shape–size relation. *J. Atmos. Oceanic Technol.,* **18,** 1773–1786.

——, V. Chandrasekar, and L. Baldini, 2006: Correction of X-band radar observation for propagation effects based on the self-consistency principle. *J. Atmos. Oceanic Technol.,* **23,** 1668–1681.

——, ——, and ——, 2008: Microphysical retrievals from dual-polarization radar measurements at X band. *J. Atmos. Oceanic Technol.,* **25,** 729–741.

Illingworth, A. J., and T. M. Blackman, 2002: The need to represent raindrop size spectra as normalized gamma distributions for the interpretation of polarization radar observations. *J. Appl. Meteor.,* **41,** 286–297.

Joss, J., and A. Waldvogel, 1990: Precipitation measurements and hydrology. *Radar in Meteorology,* D. Atlas, Ed., Amer. Meteor. Soc., 577–606.

Kalogiros, J., M. N. Anagnostou, and E. N. Anagnostou, 2006: Rainfall retrieval from polarimetric X-band radar measurements. *Proc. Fourth European Conf. on Radar in Meteorology and Hydrology,* Barcelona, Spain, Polytechnic University of Catalonia, 145–148.

——, ——, ——, M. Montopoli, E. Picciotti, and F. S. Marzano, 2013a: Optimum estimation of rain microphysical parameters using X-band dual-polarization radar measurements. *IEEE Trans. Geosci. Remote Sens.,* in press.

——, ——, ——, ——, ——, and ——, 2013b: Evaluation of an iterative polarimetric algorithm at X-band for path attenuation correction in rain against disdrometer data. *IEEE Geosci. Remote Sens. Lett.,* in press.

Kim, D.-S., M. Maki, and D.-I. Lee, 2010: Retrieval of three-dimensional raindrop size distribution using X-band polarimetric radar. *J. Atmos. Oceanic Technol.,* **27,** 1265–1285.

Maki, M., and Coauthors, 2008: X-band polarimetric radar network in the Tokyo metropolitan area—X-NET. *Proc. Fifth European Conf. on Radar in Meteorology and Hydrology,* Helsinki, Finland, Finnish Meteorological Institute, S3.7. [Available online at http://www.erad2010.org/pdf/POSTER/Thursday/02_Xband/11_ERAD2010_0354_extended.pdf.]

Marshall, J. S., and W. McK. Palmer, 1948: The distribution of raindrops with size. *J. Meteor.,* **5,** 165–166.

Marzano, F. S., G. Botta, and M. Montopoli, 2010: Iterative Bayesian retrieval of hydrometeor content from X-band polarimetric weather radar. *IEEE Trans. Geosci. Remote Sens.,* **48,** 3059–3074.

Matrosov, S. Y., D. E. Kingsmill, B. E. Martner, and F. M. Ralph, 2005: The utility of X-band polarimetric radar for quantitative estimates of rainfall parameters. *J. Hydrometeor.,* **6,** 248–262.

Mishchenko, M. I., 2000: Calculation of the amplitude matrix for a nonspherical particle in a fixed orientation. *Appl. Opt.,* **39,** 1026–1031.

Moisseev, D. N., V. Chandrasekar, C. M. H. Unal, and H. W. J. Russchenberg, 2006: Dual-polarization spectral analysis for retrieval of effective raindrop shapes. *J. Atmos. Oceanic Technol.,* **23,** 1682–1695.

Montopoli, M., F. S. Marzano, and G. Vulpiani, 2008a: Analysis and synthesis of raindrop size distribution time series from disdrometer data. *IEEE Trans. Geosci. Remote Sens.,* **46,** 466–478.

——, ——, ——, M. N. Anagnostou, and E. N. Anagnostou, 2008b: Statistical characterization and modeling of raindrop spectra time series for different climatological regions. *IEEE Trans. Geosci. Remote Sens.,* **46,** 2778–2787.

Nash, J. E., and J. V. Sutcliffe, 1970: River flow forecasting through conceptual models part I—A discussion of principles. *J. Hydrol.,* **10,** 282–290.

Ogden, F. L., H. O. Sharif, S. U. S. Senarath, J. A. Smith, M. L. Baeck, and J. R. Richardson, 2000: Hydrologic analysis of the Fort Collins, Colorado, flash flood of 1997. *J. Hydrol.,* **228,** 82–100.

Park, S.-G., M. Maki, K. Iwanami, V. N. Bringi, and V. Chandrasekar, 2005: Correction of radar reflectivity and differential reflectivity for rain attenuation at X Band. Part I: Theoretical and empirical basis. *J. Atmos. Oceanic Technol.,* **22,** 1621–1632.

Ryzhkov, A. V., and D. Zrnić, 1996: Assessment of rainfall measurement that uses specific differential phase. *J. Appl. Meteor.,* **35,** 2080–2090.

Testud, J., E. Le Bouar, E. Obligis, and M. Ali-Mehenni, 2000: The rain profiling algorithm applied to polarimetric weather radar. *J. Atmos. Oceanic Technol.,* **17,** 332–356.

Vivekanandan, J., G. Zhang, and E. Brandes, 2004: Polarimetric radar estimators based on a constrained gamma drop size distribution model. *J. Appl. Meteor.,* **43,** 217–230.

Vulpiani, G., S. Giangrande, and F. S. Marzano, 2009: Rainfall estimation from polarimetric S-band radar measurements: Validation of a neural network approach. *J. Appl. Meteor. Climatol.,* **48,** 2022–2036.

Zhang, G., J. Vivekanandan, and E. Brandes, 2001: A method for estimating rain rate and drop size distribution from polarimetric radar measurements. *IEEE Trans. Geosci. Remote Sens.,* **39,** 830–841.